Mechanical Systems and Signal Processing 146 (2021) 107039

Contents lists available at ScienceDirect

Mechanical Systems and Signal Processing

journal homepage: www.elsevier.com/locate/ymssp

A dynamic vehicle-bridge model based on the modal identification results of an existing EN57 train and bridge spans with non-ballasted tracks

Marek Szafrański

Gdańsk University of Technology, Faculty of Civil and Environmental Engineering, Department of Rail Transportation and Bridges, Narutowicza 11/12, 80-233 Gdańsk, Poland

ARTICLE INFO

Article history:
Received 16 January 2020
Received in revised form 28 May 2020
Accepted 3 June 2020

Keywords:
Bridge-vehicle interaction
Railway loads
Modal identification
FEM
Structural dynamics

ABSTRACT

This paper addresses the methodology of the bridge-vehicle dynamic model definition based on the free response measurements of an existing train and existing bridge spans. In the case of the railway vehicle, the methodology uses the impulse excitations of a single car by means of the wedge method. In the case of the bridge spans, free responses are collected after the passages of trains. The global modal parameters (frequencies and modal damping) of both structures are identified using two modal identification techniques, i.e., the eigensystem realization algorithm (ERA) and the peak picking method (PP). A simplified single-suspension model of the vehicle with 11 global dof's is proposed that can be useful in the bridge-vehicle interaction analysis. Two steel spans having non-ballasted tracks are the bridge structures. Field tests are conducted to identify the modal parameters and validate the numerical models. Finally, numerical simulations of the train passing over the bridges are compared with the in situ measurements performed under operating conditions.

1. Introduction

The bridge-vehicle dynamic interaction is an important part of design and research work, particularly for high-speed railways. When a railway vehicle passes over a bridge span, there exists a mutually coupled dynamic system in which the interaction forces between the vehicle and the bridge are induced at the wheel-rail contact area and are transmitted through the railway track. Thus, an accurate description of the bridge-track-vehicle interaction requires consideration of many complex issues with respect to the railway vehicle, railway track and bridge structural mechanics. Furthermore, the real dynamic parameters (mass, stiffness and damping) should be involved. The above situation causes basic difficulties in dynamic modelling and requires frequent simplifications. On the other hand, the degree of model complexity depends on the purpose of the analysis. If the global quantities are the main interest, the developed models do not need to be structurally complex and detailed. However, for objective results and conclusions they should always concern the real dynamic parameters. Such parameters can only be experimentally determined. Such an approach has been applied in the presented study. A simplified finite element (FE) bridge-vehicle interaction model is developed that can be useful in the dynamic analysis of bridges undergoing moving loads. The model is validated based on the modal identification results (frequencies, damping ratios and mode shapes) of the real structures – the railway vehicle and the bridge span. Both structures were tested in the natural

E-mail address: mszafran@pg.edu.pl

https://doi.org/10.1016/j.ymssp.2020.107039
0888-3270/

scale. The methodology (assumptions, mechanical and FE models definition, estimation of dynamic parameters) is universal and can also be applied to other conventional rolling stock and bridge spans to generate the bridge-vehicle dynamic simulations. This is the main objective of the presented study.

Railway vehicle testing is carried out during the approval process of the designed vehicles and to assess their technical condition. Despite advanced computer simulation capabilities, both the laboratory and track tests in the natural scale are still relevant as they are the only objective confirmation of the results. Static and dynamic tests of the completed vehicles as well as their single components are performed.

Static tests are usually performed in the specialist laboratories as the one of the obligatory steps of the vehicle acceptance procedures. Wheel unloading on a twisted track, bogie rotational resistance and sway tests are performed to assess the vehicles resistance to derailment and gauging [1,2]. The data are also used for the validation of the vehicle theoretical models. Operating vehicle dynamic tests in the laboratory conditions are frequently assessed using roller rigs [3,4]. The wheel-rail interaction and wear as well as the running stability and comfort can be tested using dedicated excitations or by simulating real on-track conditions. Additionally, extreme conditions can be evaluated, such as running close to the derailment limit can be simulated, that are impossible from the safety point of view during track tests. Track tests are conducted as the final stage of the rolling stock certification to verify the vehicle's behaviour under operating conditions [2,5,6,7]. This is an important stage from the running stability and safety point of view, because numerical simulations and even laboratory tests always have uncertainties.

One special role of railway vehicle testing is the identification of structural parameters. Regarding the dynamic values, these parameters are the mass and inertia of the bodies and the stiffness and damping of the suspensions. The parameter identification basically aims to validate the numerical models that are used in, e.g., bridge-vehicle interaction analysis. The results, as a set of reference values, can also be used in vehicle diagnostics. Changes of the identified values may indicate wear or failure in a vehicle's suspension and may identify the necessity of conducting maintenance or replacing a damaged component [8].

The dedicated tests of the individual suspension components (e.g., coil spring, leaf spring, air spring, hydraulic damper, etc.) allow for parametric identification and theoretical modelling of each component independently [9,10]. These results can then be used in the multi-body vehicle model definition. However, from the real bridge-vehicle interaction point of view, the resultant characteristics of the mounted vehicle rather than the single component values are important. Because of existing linkages (e.g., anti-roll bars, chain links) the resultant suspension characteristics may differ from those obtained from the individual components by even as much as approximately 20% [2]. The resulting suspension characteristics can be determined on the basis of modal testing by putting the vehicle into vibration and measuring the responses in selected sensor locations. Modal identification methods (MID) are applied to extract the modal parameters (frequencies, damping ratios, and mode shapes). An extensive classification of MID techniques due to the analysis domain (time or frequency), type of the excitation applied, and the response measured can be found in the literature [11,12]. Over the years, modal identification methods have been extensively studied and used for engineering and mechanical systems. The choice of an appropriate MID technique is affected by the type of collected data, i.e., force vibration, free vibration, or random vibration signals. Roller rig tests allow one to simulate different types of excitation but they are expensive and require specialist laboratories. For this reason, alternative methods of forcing the vibrations of the vehicle can be used instead, i.e., the resonance method, wedge method and on-track measurements. Resonance testing is based on the excitation of a vehicle by external forces (using exciters that have force measuring instrumentation) and measuring the response in selected locations [13,14]. The experimental modal analysis methods (EMA) that based on the FRF's as well as the output-only methods that use the free responses, can be applied for modal parameters identification. In the case of wedge tests, the vehicle is put into vibration by running over [15] or by falling from [16] steel wedges mounted to the railheads in selected locations depending on the given mode of vibration. The free-decay responses are measured, so output-only identification methods are used in modal identification. On-track tests result in the free responses that are assumed to be random (or partially random), and they are collected while the train is operating. Operational modal analysis (OMA) using a correlation analysis or the group of output-only subspace identification methods are also applied for system identification [17,18].

Modal identification and model validation of railway bridges is mainly based on in situ measurements. Similar modal identification techniques, both i.e., experimental and operational, are applied for modal parameters identification. Forced vibration tests with the use of controllable exciters, e.g. [19,20], as well as output-only tests based on the impact excitation, e.g. [21], passing locomotive excitation, e.g. [22–24], or ambient excitation, e.g. [25,26] are also conducted.

Numerical modelling allows to analyze structures in any various conditions, which are often difficult to introduce during in-situ or laboratory tests. Due to calculation capabilities of existing computers, it is a contemporary direction in the engineering and mechanical science. A historical development of the bridge-vehicle and bridge-track-vehicle theoretical models can be found in, e.g., [27,28]. The examples of simple models of vehicles as well as complex multi-body systems are presented. Railway track and bridge structure modelling is also discussed. Currently the dynamic analyses are frequently performed using the finite element method (FEM) based software with the numerical integration procedures implemented. The FEM modelling provide a very accurate representation of structures using beam, shell and solid elements. Spring-damper elements are used in order to model elastic connections and supports, gaps and to describe the wheel-rail interaction, e.g., [29]. A field or laboratory measurements of existing bridges and vehicles provide information of dynamic parameters and allow for model validation and updating, e.g., [30–32].

In the present study, the modal identification methodology is based on output-only, free-decay measurements. This is practical and particularly convenient because no input information is necessary, and thus, no dedicated exciters are required. In the railway vehicle case, the wedge method is used for the vibration excitation. A similar methodology was used [16] for the damping parameters identification of the metro car suspension. In this reference, the damping ratios were estimated using the logarithmic decrement method. On the basis of numerical simulations, it was also shown that the initial running velocity, which is the result of pushing the vehicle from the wedges, has a negligible influence on the identification results. In the present study, the eigensystem realization algorithm (ERA) [33] together with the peak picking (PP) method, which is based on spectral analysis [34], are used for modal parameter identification. The application of ERA to the wedge-based tests of vehicle proves to be very effective tool in modal identification. The logarithmic decrement method is used additionally for results verification. Based on the global modal parameters (frequencies, damping ratios, and mode shapes), the local resultant dynamic characteristics of the suspension (stiffness and damping coefficients) are calculated for the developed mechanical model of the vehicle. Finally, the single-suspension FE model of the vehicle is defined, which can be used in, e.g., vibration diagnostics of existing railway bridges. The model corresponds to the multi-body system having rigid bodies with concentrated masses and visco-elastic suspension. The EN57 electrical multiple unit, which is still a popular regional train in Poland, is adopted as the research facility. This research was performed inside the service hall of the Polish State Railways Fast Urban Railway in Tricity Sp. z o.o. (PKP Szybka Kolej Miejska w Trójmieście Sp. z o.o.) in Gdynia (Poland).

Both bridge spans under consideration are relatively simple structures having non-ballasted tracks. This is an intentional assumption because it eliminates a number of difficult to identify unknowns (particularly related to the track) and because it allows for better verification and evaluation of the developed bridge-vehicle model. The vibrations of the span are excited by the moving train. The free responses for the ERA and PP are collected after the train passes. The identified modal parameters are used in the FE model validation in terms of the mass, stiffness and damping. The final evaluation of the developed bridge-vehicle model is based on in situ measurements obtained during operating conditions. Both bridges are tested under moving EN57 trains. The displacement and acceleration signals are obtained and compared with the results of the numerical simulations in the field of forced vibrations range.

2. Materials and methods

2.1. The EN57 train – Description and testing

The EN57 trains were manufactured between 1962 and 1994 and belong to the largest series of trains in the world. Despite their aged construction, they are still one of the most popular regional trains in Poland. Many of the existing units have been modernized after 1994 (Fig. 1a).

The basic DMD configuration consists of one motor car, M, and two driving cars, D, is shown in Fig. 2. The cars are connected through the couplers. The mechanical construction features of each car are similar to those of most conventional railway vehicles. The basic differences deal with the existence of a swing-beam between the car-body and the bogie and the lack of bogie yaw dampers that assure bogie stability with respect to hunting (Fig. 1b). Both levels of suspension (primary and secondary) consist of passive components. The primary suspension consists of four coil springs and two leaf springs (for one wheelset), while the secondary suspension consists of six coil springs and two hydraulic dampers (for each bogie). The swing-beam is articulated with the car-body and supported on the bogie frame through the secondary suspension, the cradle and the coupling link. The construction of motor car M is symmetrical (car-body, bogies). A certain discrepancy

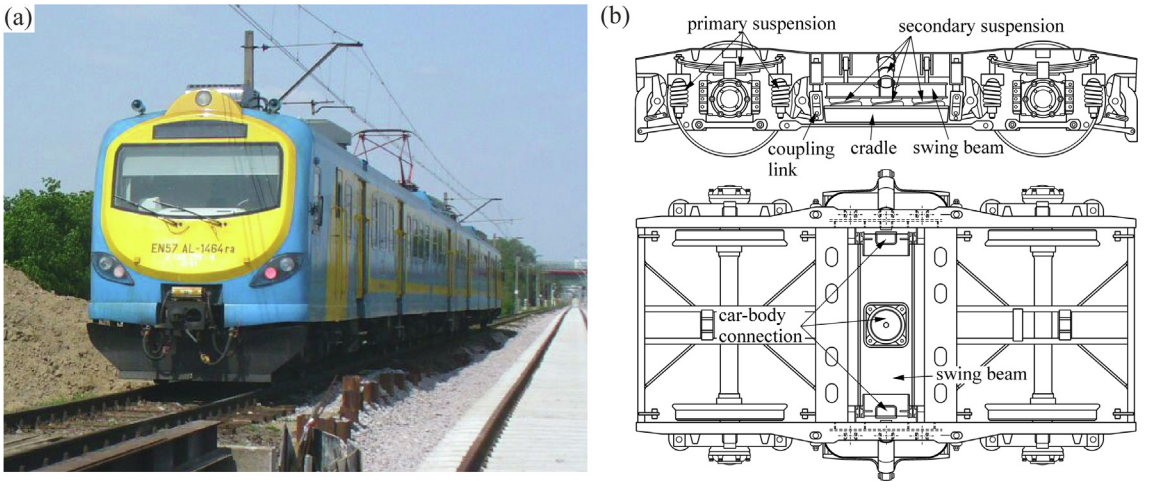

Fig. 1. The EN57 train in service (a) and the bogie construction (b).

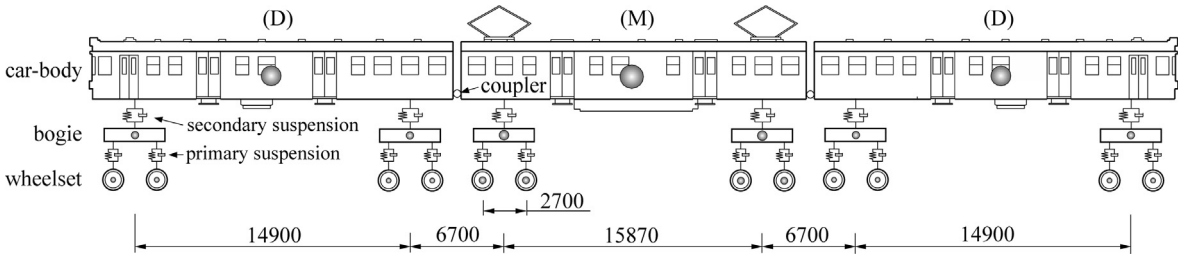

Fig. 2. The mechanical model of the EN57 train in the DMD configuration.

of the longitudinal symmetry occurs in the case of driving car D due to the driver's cab and cargo (luggage) compartment located at the single side of car-body.

To identify the modal parameters of each vehicle, stationary experiments were conducted by means of the wedge method. The experiments were carried out inside the service hall above a concrete pit, so the influence of the subgrade on the measured responses was practically eliminated. A single driving car was tested, and the free-decay responses were collected. Steel wedges that were fastened to the rails and measured 26 mm high were used (Fig. 3). Acceleration signals were measured in eight directions – seven vertical (the axle box, bogie, swing beam, and car-body floor) and one horizontal (the car-body roof). Car symmetry is assumed, so measuring sensors were only installed along the vertical axis of a single bogie (Fig. 4).

Each test was performed in the following steps: (a) fixing the wedges to the rails, (b) winching and stabilizing the car on the wedges, (c) putting the car into vibration by falling from the wedges and impacting the rails – free response data collecting, (d) stripping the wedges, moving the car back and preparing for the next test. Bouncing and rolling modes were excited (Fig. 5) by the appropriate wedge locations (three tests for each mode were carried out). In the case of the bouncing mode excitation, the wedges were mounted in front of each wheel of the two bogies (eight wedges were used), whereas for the rolling mode excitation, the wedges were placed in front of the wheels on one side of each bogie (four wedges were used).

An 16-bit HBM Spider 8 measuring system was used together with ANALOG ADXL321 accelerometers clamped to the vehicle components. The accelerometer range was 50 g for the axle box, 18 g and 50 g for the bogie frame and the swing-beam, respectively, and 5 g for the car-body. The measuring device uncertainties (i.e. sensor linearity, sensor accuracy, A/D converter resolution) were estimated based on technical specification. The obtained level was considered to provide a sufficiently high accuracy of measurements. The data acquisition system was initialized to start collecting data when the vehicle was stabilized on the wedges and just before it was pushed off. Signals were collected for approximately 10 s. The sampling frequency was set at 1200 Hz, but additional signal processing allowed the reduction of this to 240 Hz (the sample averaging method was used). The criterion was a maximum 2% difference between the root mean square value (RMS) before and after the dilution.

2.2. The bridge spans – Description and testing

Two bridge spans, both the simple structures, were adopted. The first example is the 30-m-long KO30 load-relieving span. This bridge consists of a steel box structure with direct-fastening of the rails (Fig. 6). The span is supported on temporary abutments made of wood sleepers. It was incorporated into railway track No. 502 PKP SKM during the construction of a new route through the existing E65 railway embankment in Gdańsk (Poland). A brief description of the twin span incorporated in the adjacent railway track is introduced in the literature [27].

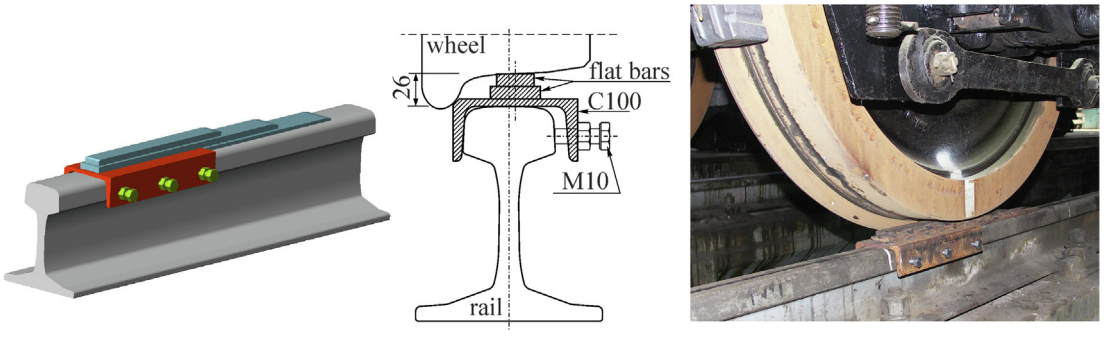

Fig. 3. Steel wedge for impulse excitation of the car.

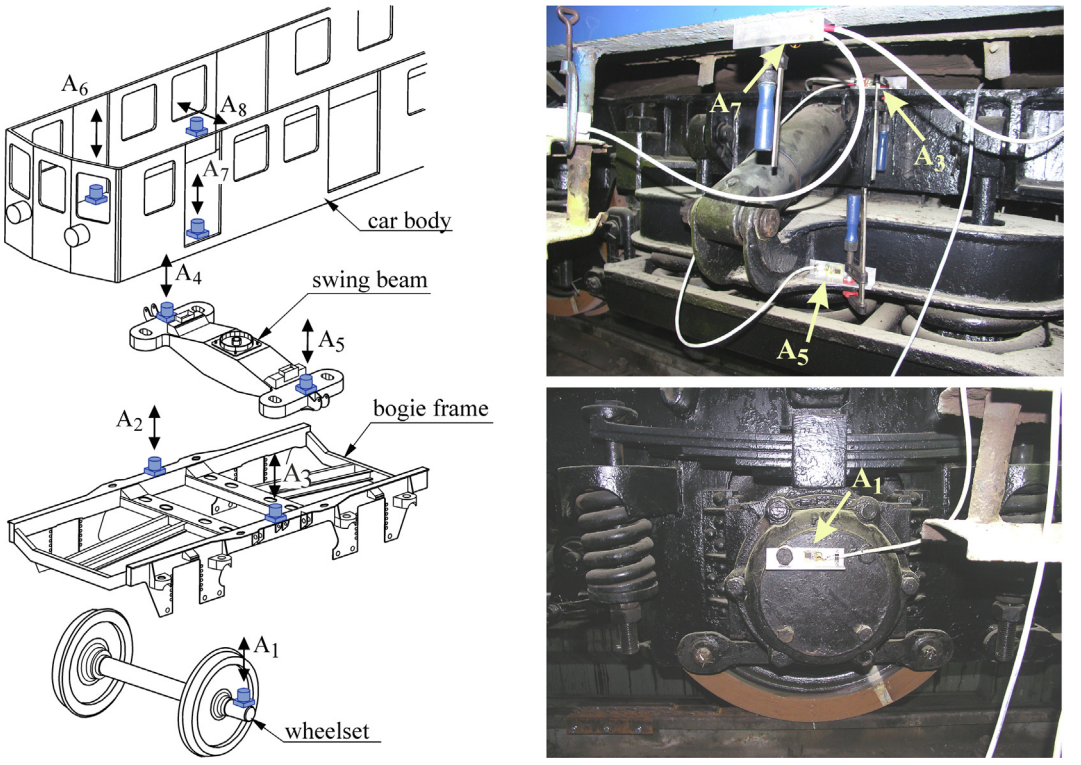

Fig. 4. Measuring sensor locations.

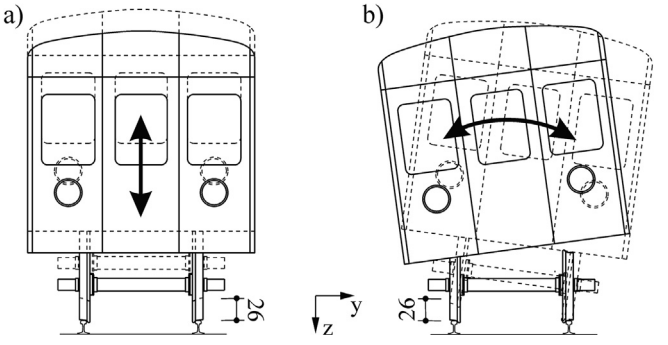

Fig. 5. Directions of vibration excitation: a) the bouncing mode, b) the rolling mode.

The second structure is the bridge over Radunia River in Gdańsk (Poland) along the E65 railway line between Warsaw and Gdynia (Fig. 7). This bridge consists of three simply supported, double-T girder open deck spans, each measuring 10.24 m long. Each span is supported on the concrete abutments through steel plain bearings. A brief description of the structure is introduced in the literature [35].

Both spans were tested during the field tests that were performed under normal operating conditions to (a) validate the numerical models based on modal parameters identification results by using free response signals determined after the train passage and (b) compare the bridge-vehicle simulation results by using forced vibration signals determined during the train passage. The vertical displacements of the mid-span as well as the vertical and lateral accelerations of the mid- and quarter-spans were measured under moving EN57 electric multiple car trains (see Figs. 6 and 7). A 16-channel, 16-bit APEK AV32AKProjekt measuring amplifier connected to a laptop was used. The accelerations were measured using APEK MA-24.01 accelerometers with the precision of 0.01 m/s^2. Displacements were measured using NOVOTECHNIK T100 potentiometric linear transducers with a precision of 0.01 mm. The sampling frequency was set at 500 Hz. Similar to the vehicle tests case, the uncertainties of measuring device were estimated. All-day measurements were taken at each span. The EN57 elec-

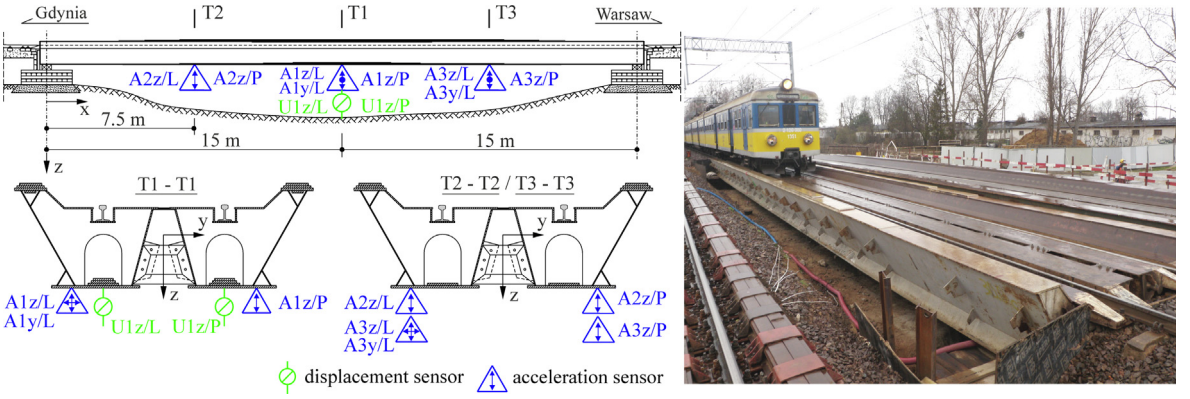

Fig. 6. The KO30 bridge with arrangement of the measuring sensors.

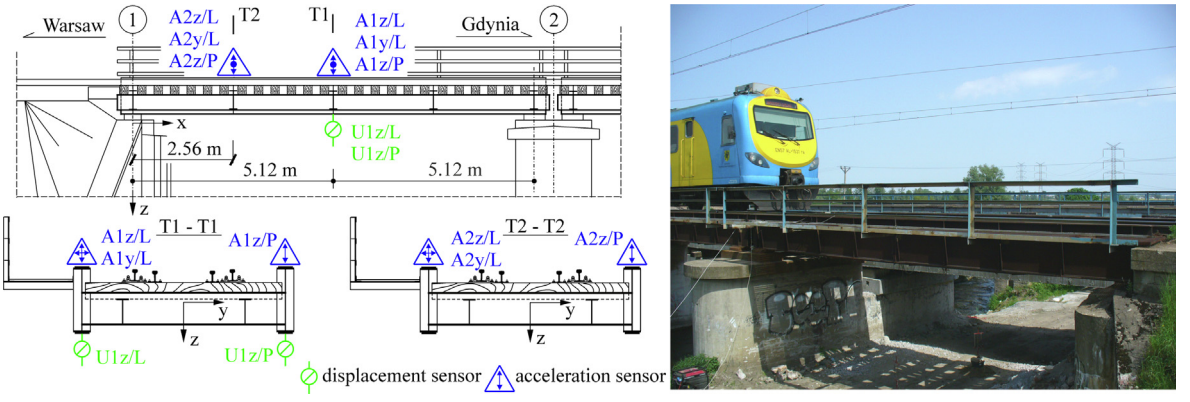

Fig. 7. The bridge over the Radunia River (external span) with the arrangement of the measuring sensors.

trical multiple car trains were operated in the DMD, DMMD and DMDDMD configurations. In the case of the KO30 bridge 19 passages were recorded, whereas 11 passages were recorded in the case of the Radunia bridge.

3. Theory/calculation

The eigensystem realization algorithm (ERA) is adopted in the present study as an effective tool for the developed research methodology. The ERA algorithm was implemented in the Matlab software [36]. This method evolves the Ho-Kalmann minimum realization problem and has been extensively studied in many identification problems in the field of mechanical systems, e.g., [37,38] and engineering structures, e.g., [39,40]. The basic principle of the ERA involves the identification of a state-space model based on the measured free-vibration responses. In this technique, the individual signal samples collected by each measuring sensor are selected to form a block Hankel matrix. The singular value decomposition of the Hankel matrix and further matrix operations allow one to estimate system matrices $\mathbf{A}^e$, $\mathbf{B}^e$, and $\mathbf{C}^e$, and then, after the transformation of the data to modal coordinates, natural frequencies, mode shapes and damping ratios.

The results of the ERA analysis are presented in frequency stabilization diagrams. For a better evaluation of the results, the averaged normalized power spectral density (ANPSD) function analysis for the set of p measured signals are plotted simultaneously:

$$\mathrm{ANPSD}(f_k) = \frac{1}{p}\sum_{i=1}^{p}\frac{\mathrm{PSD}_i(f_k)}{\sum_{i=1}^{N}\mathrm{PSD}_i(f_k)}, \tag{1}$$

where f_k is the k-th discrete frequency (k = 1, 2, . . ., N), PSD_i is the auto-power spectrum (power spectral density) of the i-th signal (i = 1, 2, . . ., p), and N is the number of discrete frequencies. The PSD function for i-th signal is obtained using the formula:

$$\mathrm{PSD}_i(f_k) = \frac{2\Delta t}{N}\left[\mathrm{FFT}_i(f_k)\right]\left[\mathrm{FFT}_i^*(f_k)\right], \tag{2}$$

where FFT_i is the fast Fourier transform of the i-th signal, and "*" indicates the Hermitian conjugation.

The modal amplitude coherence (MAC) method is additionally applied to the ERA results to distinguish the structural modes from the computational ones [41]. A MAC checks for time compatibility between the individual modal component responses of the identified model (vectors $\mathbf{q}_i^e$) and the real system (vectors $\mathbf{q}_i$) and is defined as a normalized scalar product between both vectors:

$$\mathrm{MAC}_i = \frac{\left|\mathbf{q}_i \mathbf{q}_i^{e*}\right|}{\sqrt{\left(\left|\mathbf{q}_i \mathbf{q}_i^{*}\right|\left|\mathbf{q}_i^{e} \mathbf{q}_i^{e*}\right|\right)}}. \tag{3}$$

A close to unity MAC value indicates that vectors $\mathbf{q}_i^e$ and $\mathbf{q}_i$ coincide and that the corresponding modal parameters characterize the identified system (they are classified as structural). The remaining solutions can be rejected as computational (non-physical).

Using the resultant matrices of the eigenvalue problem, $\mathbf{A}^e\mathbf{\Phi} = \mathbf{\Phi}\mathbf{\Lambda}$, the measured signals can be approximated by the theoretical responses by including only the modes that satisfy the MAC criterion. The remaining solutions (evaluated as non-physical) can be eliminated by deleting the corresponding rows and columns from matrix $\mathbf{\Lambda}$ and the corresponding columns from matrix $\mathbf{\Phi}$. The reduced matrices $\mathbf{\Lambda}^{red}$ and $\mathbf{\Phi}^{red}$ allow one to calculate the reduced, full size transition matrix $\mathbf{A}^{e,red}$:

$$\underset{(n\times n)}{\mathbf{A}^{e,red}} = \Phi^{red}\Lambda^{red}\left[\left(\left(\Phi^{red}\right)^T\Phi^{red}\right)^{-1}\left(\Phi^{red}\right)^T\right]. \tag{4}$$

Therefore, the reduced theoretical Markov parameters are as follows:

$$\underset{(p\times p)}{\mathbf{Y}_1^{red}} = \mathbf{C}^e\mathbf{B}^e, \quad \underset{(p\times p)}{\mathbf{Y}_2^{red}} = \mathbf{C}^e\mathbf{A}^{e,red}\mathbf{B}^e, \quad \ldots, \quad \underset{(p\times p)}{\mathbf{Y}_k^{red}} = \mathbf{C}^e\left(\mathbf{A}^{e,red}\right)^{k-1}\mathbf{B}^e. \tag{5}$$

The columns of the reduced Markov parameters, $\mathbf{Y}_k^{red}(:,p)$, contain the response amplitudes in the p-th sensor location for the k-th time-step corresponding only to structural modes. These responses approximate the measured signals. They are useful in the visual assessment of the correctness of the solution.

4. Results

4.1. Modal identification results of EN57 car

The free-decay responses of each individual test were collected and processed using the ERA. On the basis of convergence analysis of damping identification (the effectiveness of ERA method depends, among others, on the time range of signals included) block Hankel matrices ($\alpha p \times \beta$) are built to take into account the significant response level. The MAC criterion is set at 98%. The method parameters are assumed to be $\alpha = ap$, and $\beta = 3\alpha$, where p is number of signals and a is the value depending on the chosen signal samples (the time range of the response included in the algorithm). In the case of the bouncing excitation tests, approximately four-seconds of signals has been chosen. In the case of the rolling excitation tests, five-seconds of signals are included. These relatively short durations and the free-decay character of the response highly suit the ERA algorithm.

Considering the bouncing excitation tests, only the vertical mode and related modal parameters could be identified. In the case of the rolling excitation test, the bouncing and rolling modes are observed in the response spectrum. The results obtained from all experiments highly converge. The rolling mode frequency, f_1, lies in the range of 0.873–0.878 Hz, while the corresponding damping ratio, ξ_1, is in the range of 0.0611–0.0631. The bouncing frequency, f_2, lies in the range of 2.026–2.032 Hz, while the damping ratio, ξ_2, lies in the range of 0.0489–0.0512. The representative frequency stabilization diagram of ERA with the ANPSD function is plotted in Fig. 8 for the rolling excitation test. The rolling and bouncing modes are observed while having a MAC value greater than 99%. The corresponding modal parameters (frequencies and damping ratios) are given as the averaged values from all of the conducted tests. For the visual verification, the theoretical responses (ERA) corresponding to the identified bouncing and rolling modes are plotted in Fig. 9 together with the directly measured responses.

4.2. Railway load model definition and verification

The four-axle, single suspension mechanical model of EN57 car is developed (Fig. 10).

The model consists of lumped masses, rigid massless beams, linear springs and damper elements. The mechanical parameters of the model are summarized in Table 1. The parameters are calculated according to the following assumptions:

1. Each car is symmetrical in terms of construction, parameters and mass distribution in the both longitudinal and transverse plane.
2. The car bodies (the wheelsets, and car-body) are assumed to be rigid, the suspension characteristics are linear and they are viscously damped.

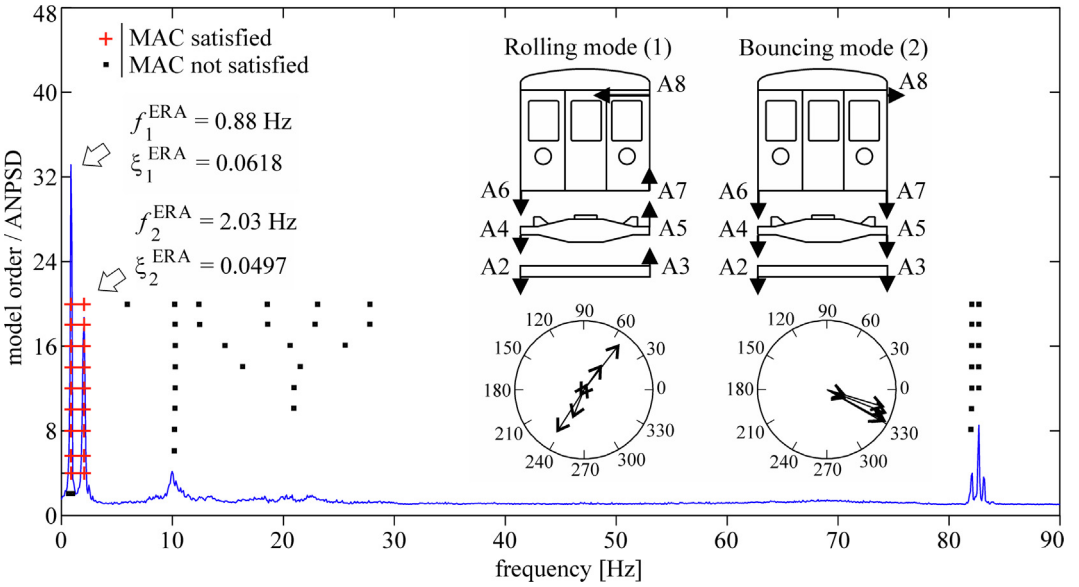

Fig. 8. Modal identification results of an EN57 driving car – rolling mode (f_1, ξ_1) and bouncing mode (f_2, ξ_2).

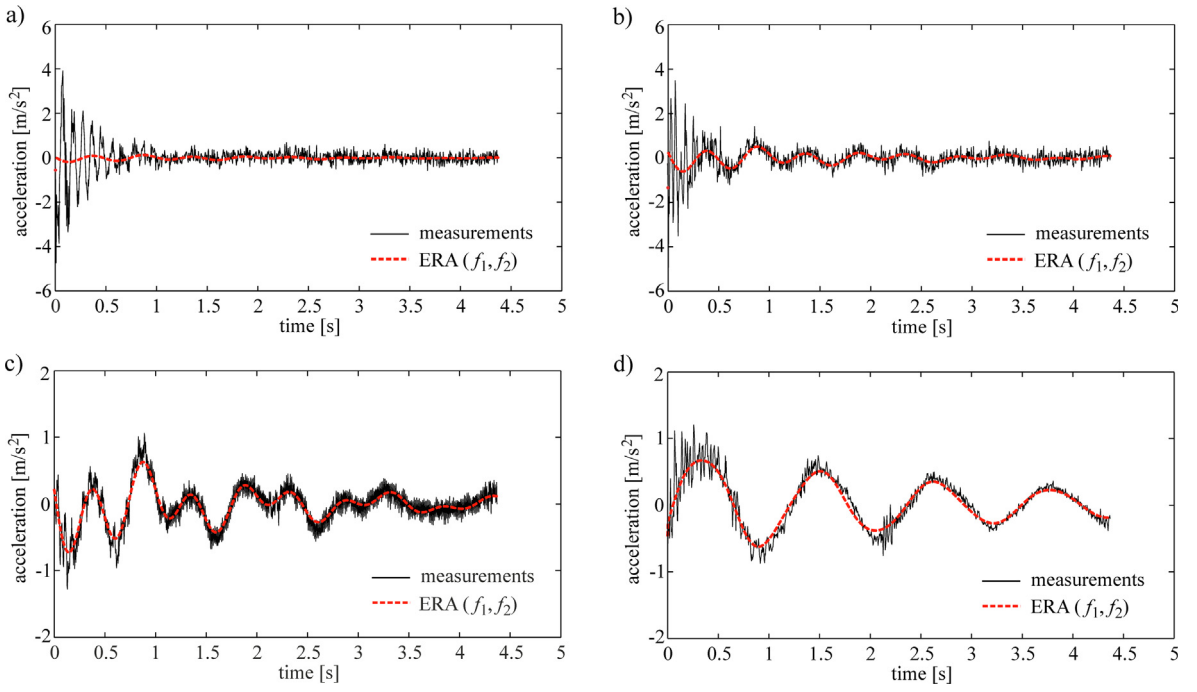

Fig. 9. The free response of an EN57 driving car during the rolling excitation test (measurements versus ERA – the reduced model of two identified modes $f_1 = 0.88$ Hz and $f_2 = 2.03$ Hz): a) bogie frame (sensor A3), b) swing beam (sensor A5), c) car body floor (sensor A7), d) car body roof (sensor A8) (sensors description according to Fig. 4).

3. The dimensions a, a_w, h_u, and h_b are taken from the technical documentation of the unit. The value of h_u represents the distance between the railhead level and the wheelset axis, while the value of h_b represents the distance between the wheelset axis and the swing beam axis.
4. The value of h_s represents the distance between the swing beam axis and the car body centre of gravity. Its value is determined by comparing the identified frequency and the numerical rolling frequency that is the result of the eigenproblem solution (both values should converge).

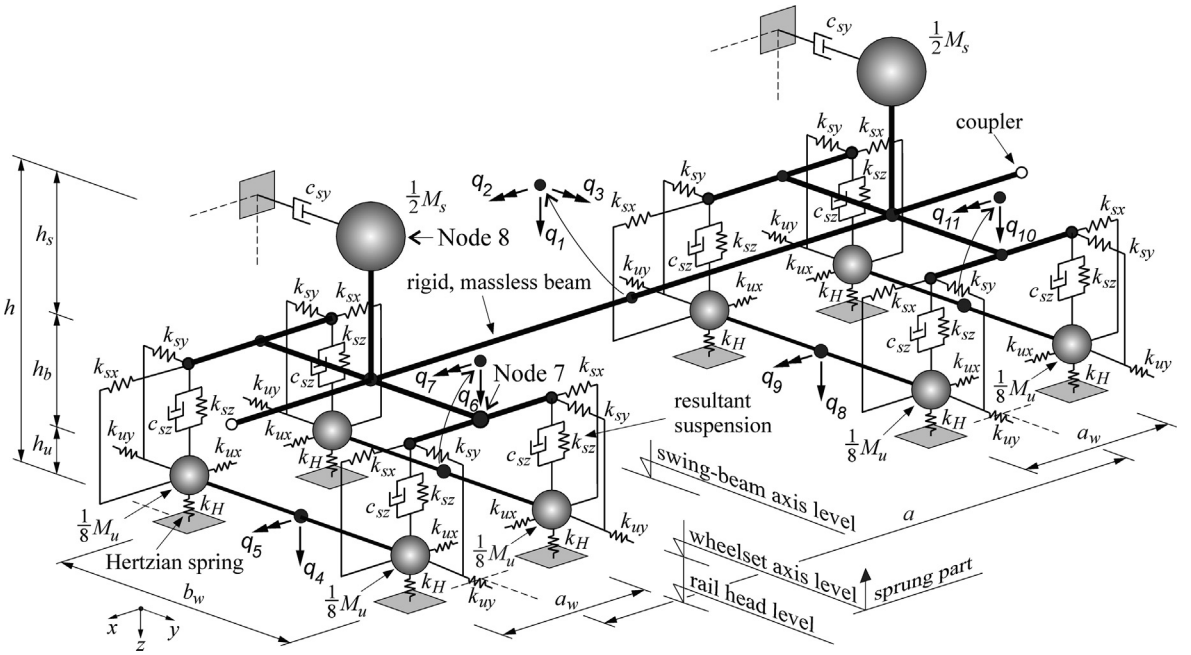

Fig. 10. The developed mechanical model of an EN57 car – single car with 11 global dof's active.

Table 1
The mechanical parameters of the EN57 unit cars.

The parameter designation	The parameter value	
	Car D	Car M
a (m)	14.90	15.87
a_w (m)	2.70	2.70
b_w (m)	1.435	1.435
h_u (m)	0.47	0.47
R (m)	0.47	0.47
h_b (m)	0.076	0.076
h_s (m)	1.625	1.625
M_s (t)	28.720	50.12
M_u (t)	5.28	6.88
M_p (t)	4.96	7.68
k_{sx}, k_{sy} (kN/m)	2×10^9	2×10^9
k_{sz} (kN/m)	583.47	1018.22
c_{sy} (kNs/m)	6.2104	10.8378
c_{sz} (kNs/m)	4.5493	7.93905
k_{ux}, k_{uy} (kN/m)	2×10^9	2×10^9
F_i (kN)	47.8	79.3
k_H (kN/m)	1.167×10^6	1.382×10^6
κ (–)	1.07	1.07

5. Only bouncing, rolling and pitching motions are allowed according to the identified modes. The pitching mode is activated due to linearity and symmetry assumption (the modal characteristics, i.e., frequencies and damping ratios, of the both pitching and bouncing modes are equal).
6. The lateral and longitudinal displacements are blocked by the use of spring elements of 'very large' stiffness values for k_{sx}, k_{sy}, k_{ux}, and k_{uy}.
7. The sprung mass, M_s, is the structural mass of the car excluding the unsprung mass of the wheelsets, M_u.
8. Both types of cars (motor and driving) have the same dynamic responses – the modal parameters of both types of cars are equal.
9. The vertical stiffness, k_{sz}, and the vertical damping coefficient, c_{sz}, are calculated based on the results of the second identified mode:

$$k_{sz} = \frac{(2\pi f_2)^2 M_s}{8}, c_{sz} = \frac{\xi_2 c_{sz}^{crit}}{8} = \frac{\xi_2 2 M_s (2\pi f_2)}{8}, \tag{6}$$

where c_{sz}^{crit} is the critical damping coefficient.

The lateral damping coefficient, c_{sy}, is calculated as:

$$c_{sy} = \kappa\left(\frac{c_{sy}^{tot}}{2} - c_{sy(z)}\right), \tag{7}$$

where $c_{sy}^{tot} = \xi_1 2M_s(2\pi f_1)$ is the total lateral damping related to the first identified mode, $c_{sy(z)}$ is the lateral damping component related to the activity of the vertical dampers and κ is the correction factor. Assuming that the rolling motion occurs around the centre of gravity of the swing beam (Fig. 11), the value of $c_{sy(z)}$ can be calculated from the sum of moments relative to point A:

$$c_{sy(z)}(h_s\tan\alpha)h_s = 4c_{sz}\left(\frac{b_w}{2}\tan\alpha\right)\frac{b_w}{2} \Rightarrow c_{sy(z)} = \frac{c_{sz}{b_w}^2}{{h_s}^2}, \tag{8}$$

The Hertz theory of elastic contact between two cylinders is adopted to describe the vertical wheel-rail interaction [42]. The equivalent nonlinear contact spring is applied between the wheel and the rail with the Hertz law:

$$F_i = c_H {u_i}^{3/2}, \tag{9}$$

where F_i [N] and u_i [m] are the vertical interaction force and the vertical shortening, respectively, between the i-th wheel and the rail in contact, and c_H is the Hertzian nonlinear spring stiffness [N/m$^{3/2}$]. Since the dynamic shortening is small, a linearized Hertzian spring, k_H, [N/m] can be used instead. The value of k_H can be calculated as the secant stiffness around the static wheel load [43]:

$$k_H = \frac{dF_i}{du_i} = \frac{3}{2}c_H {u_i}^{1/2} = \frac{3}{2}{c_H}^{2/3}{F_i}^{1/3} = \frac{3}{2}G^{-1}{F_i}^{1/3}. \tag{10}$$

The value of $G = {c_H}^{-2/3}$ [m/N$^{2/3}$] is the Hertzian flexibility constant. In the literature [44] the value of G is determined as a function of wheel radius, R, and the rate of wear and tear: $G = 4.57R^{-0.149} \times 10^{-8}$ [m/N$^{2/3}$] for a new wheel and $G = 3.86R^{-0.115} \times 10^{-8}$ [m/N$^{2/3}$] for a worn wheel. Similar to the reported method [45], the averaged value of G is assumed for the k_H calculations.

The mass of the passengers, M_p, is also added to the structural mass of each car but is activated only in the bridge-vehicle interaction analysis. The number of passengers is set as the number of seats and human is assumed to weigh 80 kg. Therefore, the total static value of the vertical force $F_i = 1/8(M_s + M_u + M_p)g$ is taken for the k_H Hertzian stiffness calculation, where g [m/s^2] is the acceleration of gravity.

Following the development of the mechanical model of the vehicle, a three-dimensional FE model is defined using the commercial SOFiSTiK software [46] (Fig. 12a). The model consist of mass points (concentrated masses acting in the centre of gravity of an individual car element), linear spring elements (the resultant suspension), rigid car body elements (massless beams holding the sprung masses supported by the car suspension) and rigid wheelset axle elements (massless beams holding the unsprung masses supported by the Hertzian contact springs). Each suspension spring is characterized by the vertical and horizontal stiffness coefficients, k_{sz}, k_{sx}, k_{sy}, and the vertical damping coefficient, c_{sz}. The horizontal car body spring acting in the mass point is characterized by the lateral damping coefficient, c_{sy}. The contact wheel-rail Hertzian spring is assumed to be double-sided (no wheel-rail separation is possible) and it is characterized by the vertical and horizontal stiffness coeffi-

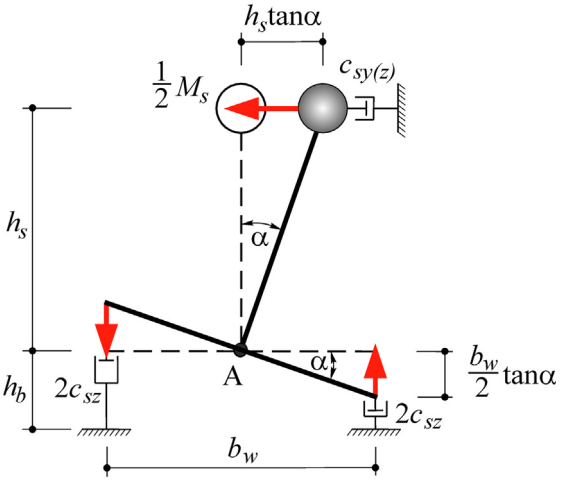

Fig. 11. The assumed rolling mode kinematics for the $c_{sy(z)}$ calculations.

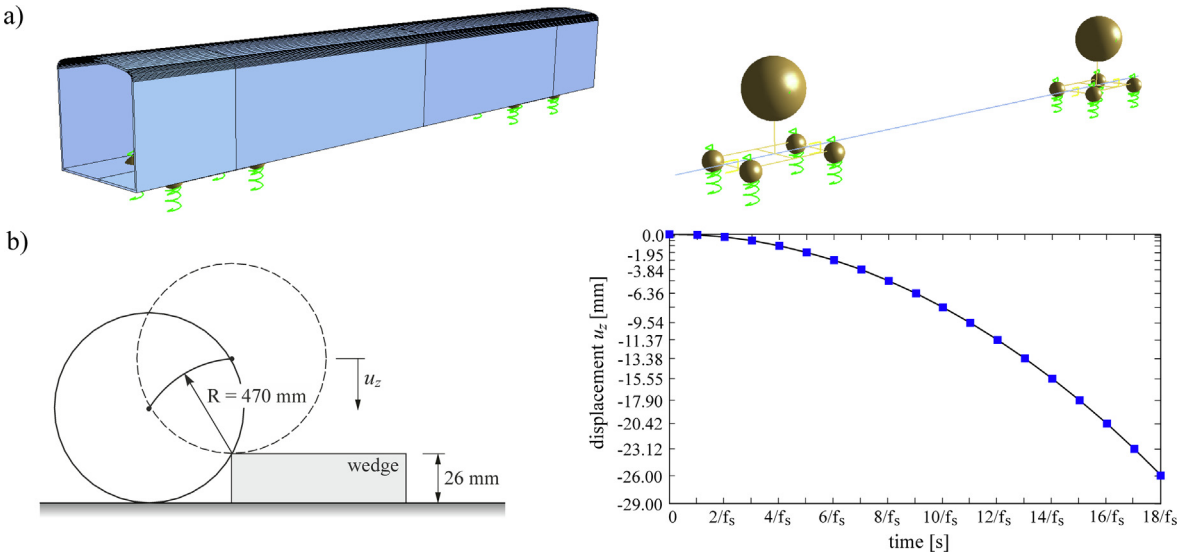

Fig. 12. (a) The developed FE model of a railway vehicle, (b) the dropping trajectory and vertical excitation curve of the wheelset nodes in the wedge simulations (f_s = 240 Hz).

cients, k_H, k_{ux}, k_{uy}. To verify the model, the wedge tests have been simulated according to the experimental conditions. The compatibility between the measured and numerical modal parameters (frequencies and damping ratios) is assumed to be the verification criterion. An impulse excitation is applied in the form of a vertical displacement in time to the wheelset nodes. A portion of a circular arc with a radius of 470 mm is assumed to be the dropping trajectory (Fig. 12b). The bouncing and rolling modes are excited and the responses are collected in node no. 7, which corresponds to the A7 sensor and in node no. 8, which corresponds to the A8 sensor (see Figs. 4 and 10). The Newmark-β integration procedure is used with the parameter values of $\beta = 1/4$ and $\gamma = 1/2$ and a sampling frequency, f_s, of 240 Hz. A comparison of the measured and numerical responses in the time and the frequency domains is presented in Fig. 13. The results highly converge in phase, frequency and decrement of damping (for both bouncing and rolling modes). Only the numerical bouncing amplitudes of the carbody (node 7) are greater than measured amplitudes. However, due to the numerical model simplifications and approximate excitation conditions, this particular difference has been accepted and the compatibility between frequencies and damping ratios has been recognized as the verification criterion. In Fig. 14 the individual numerical mode responses and the corresponding modal parameters are shown. The damping ratios are calculated using the logarithmic decrement method. By comparing with the measured values (Fig. 8), one can see that both results converge. The frequencies are consistent, while the damping ratios differ by 0.6% in the case of the rolling mode and by 1.1% in the case of the bouncing mode.

4.3. Modal identification and FE model validation of the bridge spans

The free acceleration responses collected after the passages of trains have been processed using the ERA and PP techniques to extract the modal parameters. The representative frequency stabilization diagrams of the ERA together with the plotted ANPSD functions are shown in Fig. 15. Only the first bending mode has been successfully identified for both structures due to the type of applied excitation. The corresponding modal parameters, i.e., the frequencies and damping ratios are also listed.

The FE models have been developed using the SOFiSTiK software (Fig. 16). The global stiffness of a span depends on the Young modulus of the material, E, and the cross-section of the structural elements. The global mass depends on the unit weight of the main structural elements as well as the second-order elements (e.g., the vertical ribs, the angle plates) and non-structural elements (e.g., the railway track, the sidewalk) that are not included in the beam models.

The global stiffness of the model is assumed to be correctly defined since the material properties (E = 205 GPa) and geometry of the structure are taken from the technical documentation and the field inventory measurements. To ensure the compatibility between the measured and numerical frequencies, the theoretical unit weight of steel is increased due to second-order and non-structural masses. In the case of the KO30 bridge (direct fastening of the rails) a 12% increase is applied, while in the case of the Radunia bridge an 18% increase is applied (mainly due to the weight of the railway track). The stiffness proportional damping model, $\mathbf{C} = b\mathbf{K}$, with the proportionality factor, $b = \xi_1/\pi f_1$, is assumed. To verify the correctness of the damping assumption, an impulse excitation as well as the moving force excitation have been applied to the model and the free mid-span responses have been collected. The numerical damping ratio is calculated using the logarithmic decrement (LDD) technique. The relationship, $\mathrm{LDD} = 2\pi\xi_1$, is applied. The results of modal identification and model validation are summarized in Table 2. The relative difference of the damping ratio between the measured and numerical responses of the

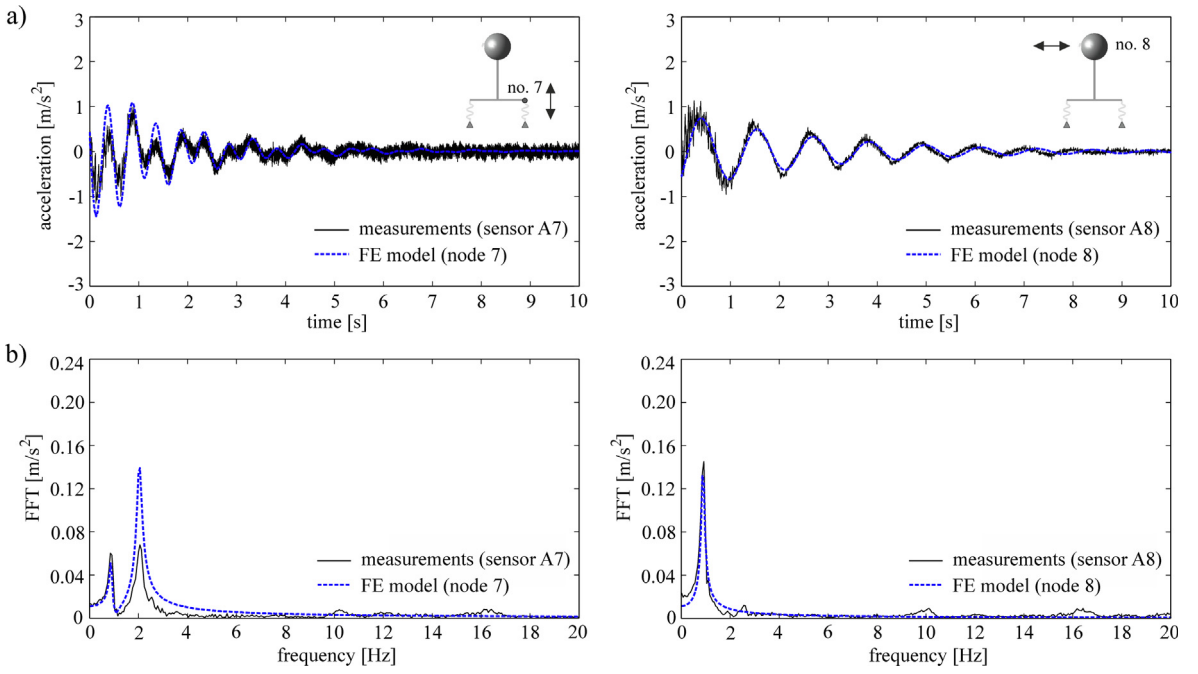

Fig. 13. The free response of an EN57 car (rolling mode excitation) – measurements versus simulations, (a) comparison in the time domain, (b) comparison in the frequency domain.

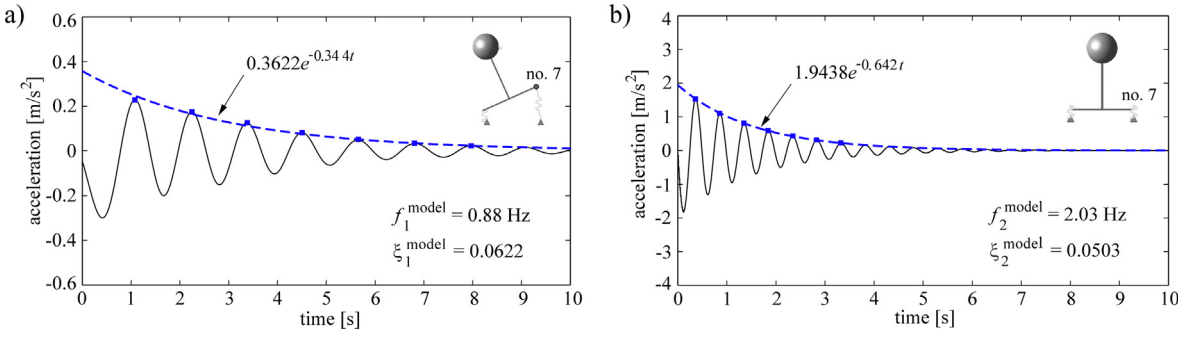

Fig. 14. Simulation results of the wedge tests, (a) rolling mode characteristics – rolling excitation (filter range 0.1–1.1 Hz), (b) bouncing mode characteristics – vertical excitation.

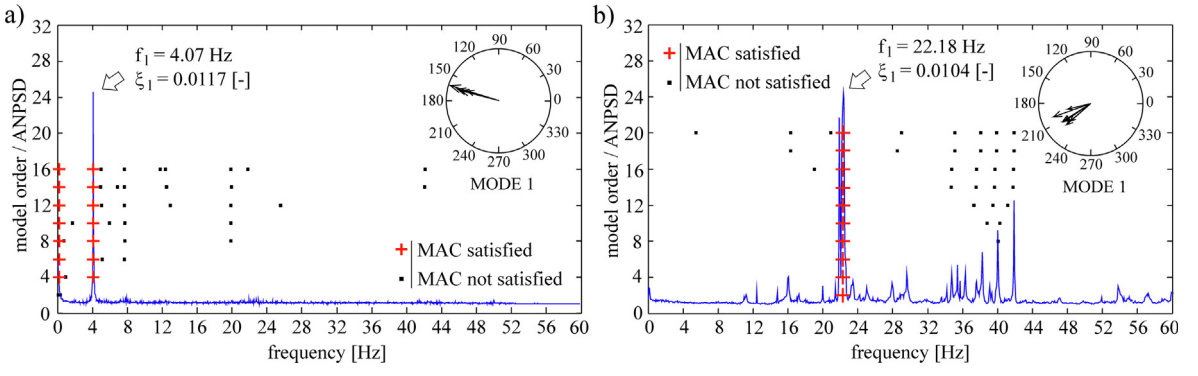

Fig. 15. The frequency stabilization diagrams of the ERA with the ANPSD functions, (a) the KO30 bridge, (b) the bridge over Radunia River.

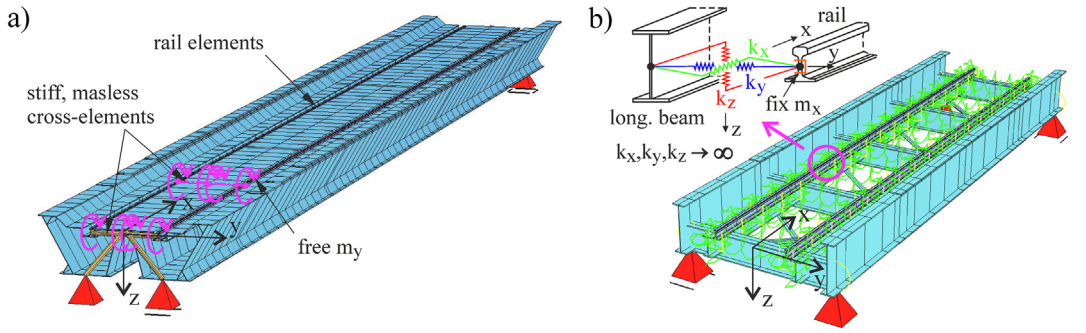

Fig. 16. The FE models of two bridge spans (SOFiSTiK): (a) the KO30 bridge, (b) the bridge over the Radunia River.

Table 2
Results of the model validation – dynamic parameters of the considered bridge spans.

Bridge span/parameter	Measurements			FE model			
	f_1^{ERA} [Hz]	ξ_1^{ERA} [–]	LDD^{ERA} [–]	f_1^{FEM} [Hz]	b ($\mathbf{C} = b\mathbf{K}$)	LDD^{FEM} [–]	ξ_1^{FEM} [–]
KO30 Bridge	4.07	0.0117	0.0735	4.06	$9.150 \cdot 10^{-4}$	0.0779	0.0123
Radunia Bridge	22.18	0.0104	0.0653	22.20	$1.492 \cdot 10^{-4}$	0.0697	0.0109

KO30 bridge is 4.9%, while that of the Radunia bridge is 4.6%. The frequencies are consistent. The railway track is modelled in the substitution manner. Only the rails are considered to be the structural finite elements. In the case of the Radunia bridge, the wood sleepers and checkrails are considered to be static loads. The connection between the rails and the longitudinal beams is assumed to be rigid. Spring elements having large stiffness values are used between the corresponding nodes (see Fig. 16).

4.4. The vehicle-bridge interaction analysis

Numerical simulations of a train passing over the bridge are carried out using the SOFiSTiK software with the direct Newmark-β integration procedure implemented. According to the convergence analysis, the time-step is set at $\Delta t = 0.004$ s in the case of the KO30 bridge and $\Delta t = 0.002$ s in the case of the Radunia bridge. The bridge-vehicle interaction is provided by contact moving spring elements acting in the wheel nodes and by contact nodes of the bridge structure. The springs are described by the Hertz law. The position of the train changes over time depending on the given time step and moving velocity. Interaction forces are calculated based on the current deformation of the system – relative displacement between moving train (wheel mass points) and the deformed bridge structure. The solving procedure implemented in the software was verified [47] on the basis of the concentrated force and single-mass oscillator models moving on a Euler-Bernoulli beam. In the present study, the developed dynamic model of an EN57 train, as well as the series of moving forces model, are used in the simulations (Fig. 17). The numerical results are compared with the in situ measurements. The following basic assumptions are made in the numerical simulations:

a) the train moves at a constant speed on a straight and non-deformable track,
b) the support conditions of the bridge are assumed to be rigid,
c) only the vertical wheel-rail interaction (normal problem) is taking into account and the vertical bridge-vehicle vibrations are considered.

A comparison of the measured and numerical results in the time domain is shown in Fig. 18 for the vertical displacements and in Fig. 19 for the vertical accelerations. In the case of the KO30 bridge, the train moves at a velocity of 26 kph in the DMMD configuration, while in the case of the Radunia bridge the train moves at a velocity of 49 kph in the DMD configuration. According to the guidelines [48], the measured acceleration signals are considered to be in the frequency range of 0 – 30 Hz for the KO30 bridge and 0 – 35 Hz for the Radunia bridge. The root mean square value (RMS) is also applied as the quantitative comparison indicator of the acceleration signals. The RMS value is calculated in the forced vibration time range, i.e., during the time that the train is on the bridge. For the KO30 bridge, vibration time range is 15.5 s, while for the Radunia bridge, it is 5.3 s. Fig. 20 shows the power spectral densities (PSD) of the acceleration records. A comparison of the measured and numerical results regarding the developed vehicle model is presented, separately for the forced and free vibration time range.

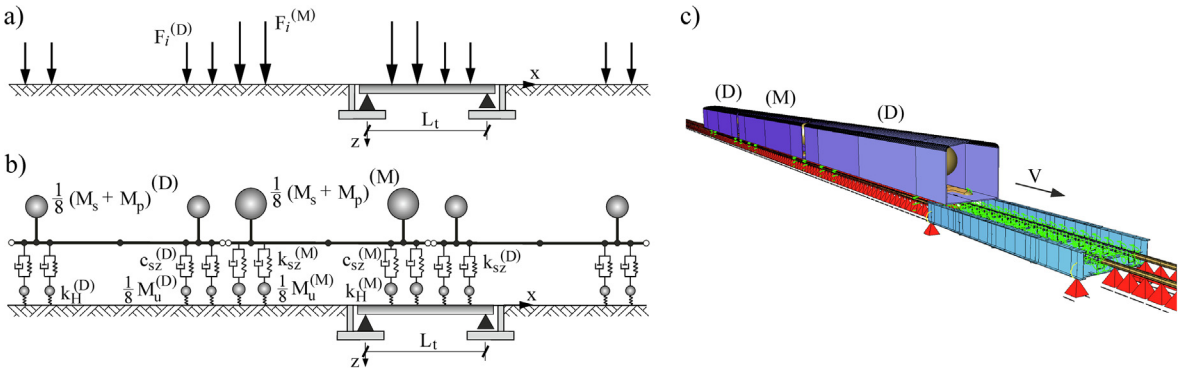

Fig. 17. The considered railway load models in the DMD configuration – side view: (a) the series of moving forces, (b) developed single suspension model, (c) visualization of the Radunia bridge-vehicle model (SOFiSTiK).

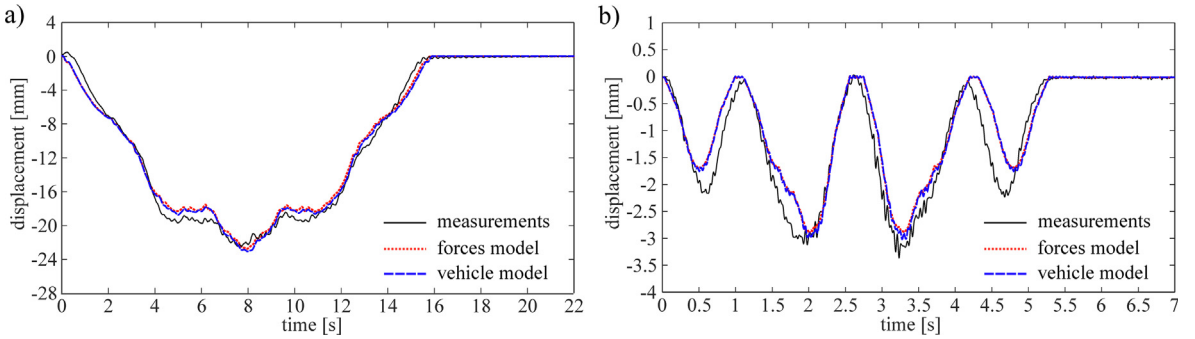

Fig. 18. Mid-span responses to a vertical displacement (measurements versus simulations): (a) passage of an EN57 train (DMMD configuration) over the KO30 bridge at a speed of 26 kph, (b) passage of an EN57 train (DMD configuration) over the Radunia bridge at a speed of 49 kph.

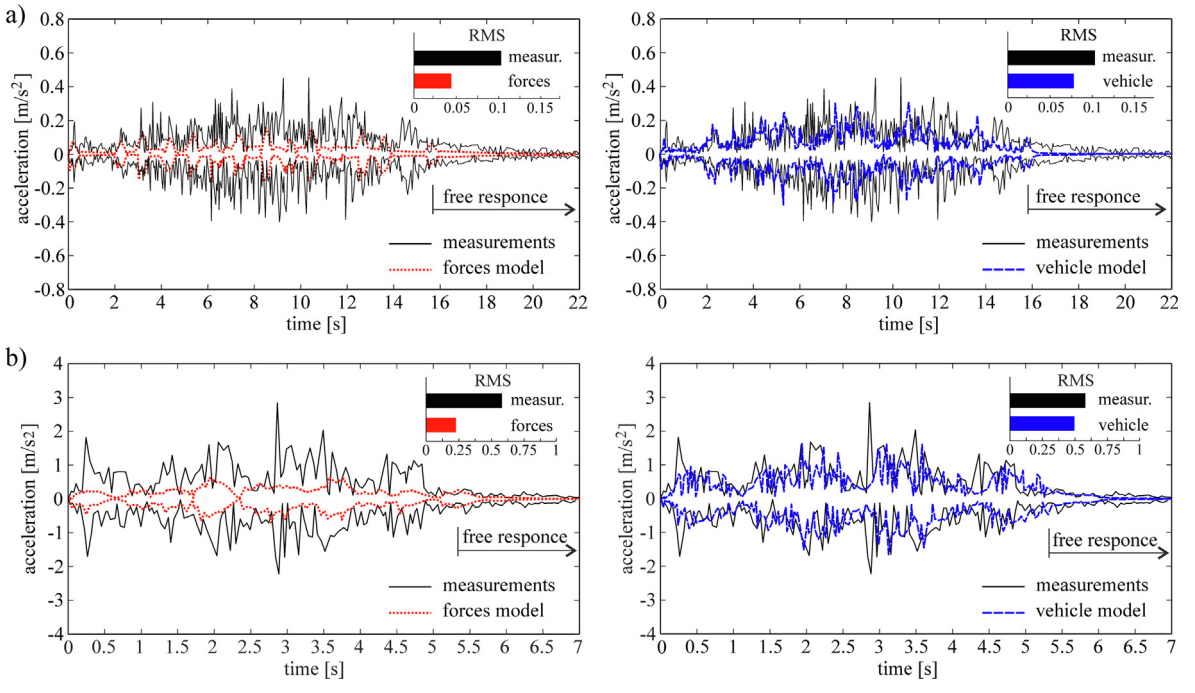

Fig. 19. The mid-span responses to a vertical acceleration (envelopes): (a) the passage of an EN57 train in the DMMD configuration over the KO30 bridge at a speed of 26 kph, (b) the passage of an EN57 train in the DMD configuration over the Radunia bridge with at a speed of 49 kph.

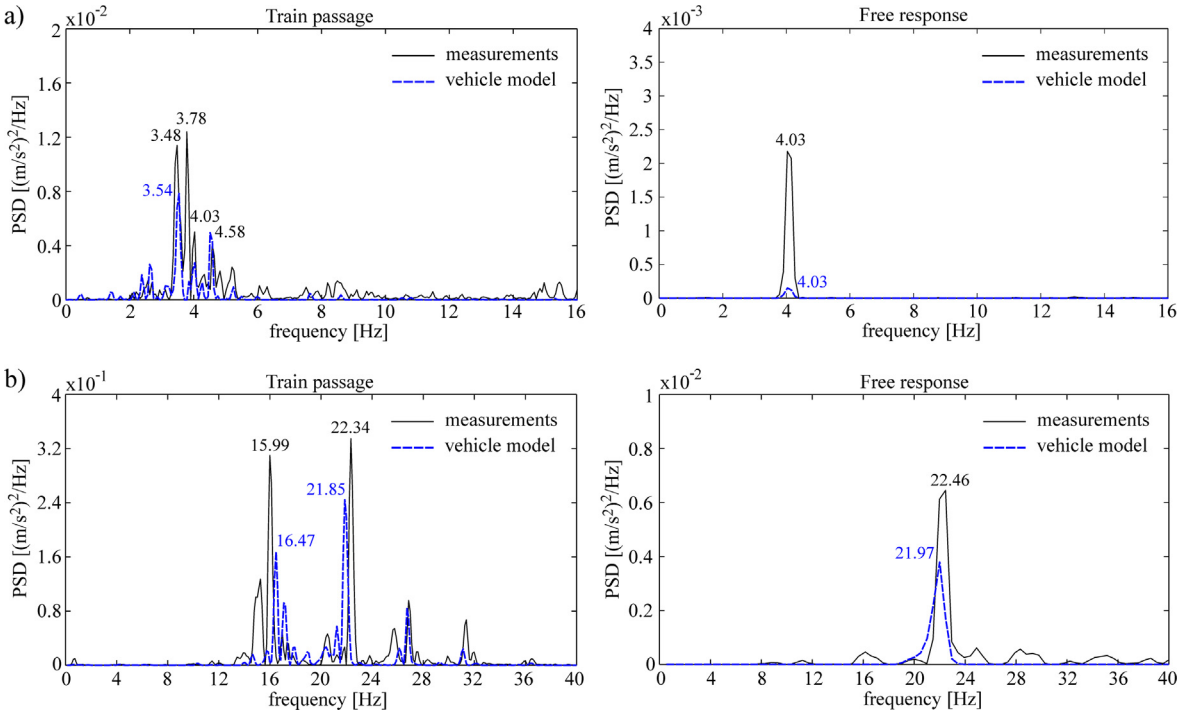

Fig. 20. A comparison between measured and numerical spectra of the acceleration records: (a) the KO30 bridge, (b) the Radunia bridge.

5. Discussion

This paper addresses the methodology of the bridge-vehicle FE model definition based on the modal identification results of an existing railway vehicle and the existing bridge spans. The methodology uses free-decay response data occurring after impulse excitation (in the vehicle case) or by immediate interruption of running excitation (in the bridge case). The wedge method used for the vehicle excitation has provided high-quality response data that fit the ERA algorithm very well. Both excited modes (bouncing and rolling) are visible in the response spectrum and the modal parameters for all conducted tests are estimated with a high level of convergence. The maximum discrepancy between the individual test results of the bouncing frequency is 0.3% while that of the rolling frequency is 0.5%. The corresponding damping ratios differ by a maximum of 4% for the bouncing mode and by a maximum of 3% for the rolling mode. The ERA-based frequency results have been confirmed using spectral analysis, while the ERA-based damping results have been confirmed using the LDD technique.

The simplified single suspension FE model of the railway car is developed having 3 car-body global modes active, i.e., bouncing, rolling and pitching. The wheelset mass is separated from the bogie mass and is assumed to be unsprung, while the remaining bogie mass is added to the car-body mass. Each wheelset has 2 active global modes, i.e., bouncing and rolling and is in full contact with the rails by the use of double-sided Hertzian springs. The suspension characteristics are calculated on the basis of the first rolling and first bouncing modal parameters. These modes are visible in all vehicle component responses (see Figs. 8 and 9). In the case of the bogie frame, an additional stable, but quickly damped local mode, having a frequency 10.23 Hz and the MAC value 96% occurs. This mode is also structural and it is the result of the presence of the secondary suspension. It stops after one second. In the case of the swing-beam, the local vibrations of a frequency of approximately 20 Hz are visible during the first 0.5 sec. However, this mode is unstable, and has a low MAC value, which is the result of existing gaps in the bumpers and between the swing-beam and the car-body. According to the linearity assumption, the existing bumpers, linkage gaps and other nonlinear effects are neglected. According to the single suspension model assumption, the bogie frame and the swing-beam are not considered to be independent structural masses.

The local dynamic characteristics of the vehicle suspension are calculated based on the identified global modal parameters. Chapter 4.2 deals with the assumptions and calculations that have been made. To verify the model, numerical wedge tests are simulated. The consistency between the measured and numerical results is 99%. Both frequency values (bouncing and rolling) as well as the vertical damping ratio have satisfied this condition directly. Only in the case of horizontal damping of the car-body has a 7% correction had to be made in relation to the directly calculated values.

Small-span and medium-span beam bridges are considered. Both spans have relatively simple structures. This structural simplicity allows for the simple modelling and facilitates the evaluation of the simulation results in comparison to the measurements. In a manner similar to that used for the railway vehicle, the bridge FE models are validated based on in situ measurements and the identified modal parameters results. The moving vehicle proved to be an effective tool in the bridge free

response excitation, however, using the ERA method, only the first bending mode could be clearly identified for both structures. The acceleration signals were used as the input data. Spectral analysis as well as the LDD technique are used for ERA-based results confirmation. The minimum consistency between measured and numerical modal parameters is 95%, which is frequently considered to be acceptable for engineering structures. Both frequencies have been validated and are consistent, while the initially calculated stiffness proportional damping model has given less than a 5% discrepancy between the measured and numerical damping ratios. The obtained level of compliance has been accepted for further studies and no additional corrections have been made. The identified damping ratios of both spans are typical for structures of that type. The research results presented in Fryba [49] for example, determined the mean value of the damping ratio of steel railway bridges (in general) to be 1.25% with a standard deviation of 0.6%.

The bridge-vehicle analysis is summarized in the undertaken study. In addition to the developed single suspension model of the vehicle, the series of moving forces model is also considered, as it is commonly used in the engineering practice. Both solutions refer to the field measurements.

The method of vehicle modelling significantly affects the quantitative acceleration results. In both cases, the comparison in the time domain as well as the RMS values show similar tendencies. The omission of the inertial forces of the load (a series of moving forces model) significantly underestimates the vibration amplitudes, while the results obtained using the dynamic model of the vehicle are much closer to the measurements. The acceleration analysis of railway bridges of similar structural types (steel beam bridges with the direct fastening of rails or with the railway track of an open type) require consideration of the dynamic modelling of the loads. The real parameters identification-based model of vehicle, at least with the single suspension level and with the separated unsprung wheelset mass, is more than adequate for the objective results evaluation.

By observing the power spectra of acceleration records, one can notice the significant influence of the vehicle existence on the frequency results. In both considered cases, the vehicle speed is low and its mass is relatively high in comparison to the mass of the bridge span. Therefore, a wide frequency range is induced during the train passage. After the train leaves the bridge, only the single frequency is visible which corresponds to the first bending mode of vibration. In general, the numerical spectra covers the dominant frequencies of the measured spectra. However, the numerical amplitudes of both considered bridges are lower than measured ones. A significant difference occurs especially in the KO30 free response. In this particular case, the considerably lower numerical amplitudes may indicate, among others, the need to adjust the real support flexibility (vertical and horizontal) of the temporary abutments. Thereby, the initial conditions of the free vibration excitation may be updated. In both bridge span cases, however, the frequency values converge to the ERA-based identification results and the FE eigenvalue solution (see Table 2).

The displacement results are less sensitive to the type of applied load. Both load models under consideration give similar results that are close to the measuring results. From the technical point of view, both models are suitable for the serviceability limit state assessment in relation to the displacement requirements. A good compatibility between the measured and the theoretical maximum displacements allows one to correctly assess the geometry and stiffness of the spans and generate a good estimation of the vehicle mass. Only in the case of the bridge over Radunia River did some discrepancies in the extreme values exist that were caused by the external bogies of the driving cars. A possible reason is the lack of longitudinal symmetry in the mass distribution of the car and an underestimation of the mass of passengers (cargo), whose number on the tested line is variable and is strongly dependent on the time of day. A value of longitudinal mass eccentricity may be verified by measuring the wheelsets loads and by identification of the pitching mode of vibration.

6. Conclusions

The objective analysis of bridges under moving loads requires the determination of the real dynamic parameters of both spans and moving vehicles. The presented methodology of a FE bridge-vehicle dynamic model definition based on modal parameters identification of existing structures, can be an effective way to increase the reliability of simulation results. Wedge-based tests are very effective methods of providing free vibration excitation of a railway vehicle. Their basic advantage is the use of high-quality data and the fact that it is uncontaminated by environmental and railway track interactions. The basic disadvantage of using wedge tests is the necessity of removing the railway vehicle from operation (the vehicle should be parked).

The discussed results prove that an ERA can be successfully applied to the developed methodology. However, in the case of bridge spans, only the first bending modes could be identified using the applied type of excitation and sensor arrangements. Regarding the identified modes, a high repeatability of the modal parameters among the individual tests has been observed.

A simple but real parameter-based structural model is assumed in the presented study. The field tests are crucial to the developed bridge-vehicle model assessment, which has been the main purpose of this work. In spite of the simplifications that have been made, the developed dynamic model of the vehicle can be useful in the global dynamic analysis of railway bridges. The presented methodology of bridge-vehicle FE model definition and validation can be successfully applied to other types conventional rolling stock vehicles and bridge spans.

This research is being further refined. The vehicle model can be upgraded by identifying additional modes of vibration (i.e., pitching, lateral and yawing) and by considering the separated masses of bogies. In this case, however, the vehicle model would be significantly expanded and different strategy of model definition should have been applied. The developed vehicle-

bridge model can be extended into a vehicle-track-bridge system by considering the real track parameters (parametric identification) as well as the track irregularity and gauge (measurements). Additionally, the wider speed ranges and bridge types may allow for more objective inference.

CRediT authorship contribution statement

Marek Szafrański: Methodology, Validation, Investigation.

Declaration of Competing Interest

The authors declare that they have no known competing financial interests or personal relationships that could have appeared to influence the work reported in this paper.

Acknowledgements

The author expresses gratitude to the Authorities and Employees of the Polish State Railways Fast Urban Railway in Tricity Sp. z o.o. (PKP Szybka Kolej Miejska w Trójmieście Sp. z o.o.) in Gdynia (Poland) for research cooperation and for the use of a railway vehicle in the testing.

References

[1] J. Stow, E. Andersson, in: S. Iwnicki (Eds.), Handbook of Railway Vehicle Dynamics, Taylor and Francis, 2006, pp. 423–456.
[2] J. Evans, M. Berg, Challenges in simulation of rail vehicle dynamics, Veh. Syst. Dyn. 47 (8) (2009) 1023–1048.
[3] W. Zhang, H. Dai, Z. Shen, J. Zeng, Roller Rigs, in: S. Iwnicki (Eds.), Handbook of Railway Vehicle Dynamics, Taylor and Francis, 2006, pp. 457–506.
[4] S. Myamlin, J. Kalivoda, L. Neduzha, Testing of railway vehicle using roller rigs, Proc. Eng. 187 (2017) 688–695.
[5] P. Dupont, Testing the dynamic behaviour of vehicles: Normalization of test conditions by use of multi linear regressions, 9th World Congress on Railway Research (WCRR), Lille 22-26 May (2011).
[6] Railway Group Standard GMRT2141, Permissible Track Forces and Resistance to Derailment and Roll-Over, June 2019.
[7] European Standard PN-EN 14363+A1:2019-02, Railway applications. Testing and Simulation for the acceptance of running characteristics of railway vehicles. Running behaviour and stationary tests, February 2019.
[8] P. Li, R. Goodall, P. Weston, Ch.S. Ling, C. Goodman, C. Roberts, Estimation of railway vehicle suspension parameters for condition monitoring, Control Eng. Pract. (Control Eng. Pract.) 15 (2007) 43–55.
[9] S. Bruni, J. Vinolas, M. Berg, O. Polach, S. Stichel, Modelling of suspension components in a rail vehicle dynamic context, Veh. Syst. Dyn. 49 (7) (2011) 1021–1072.
[10] B. Kadziela, M. Manka, T. Uhl, Validation and optimization of the leaf spring multibody numerical model, Arch. Appl. Mech. 85 (2015) 1899–1914.
[11] N.M.M. Maia, J.M.M. Silva, eds., Theoretical and Experimental Modal Analysis, Research Studies Press Ltd., Baldock, Hertfordshire, England, 1997.
[12] L. Zhang, An Overview of Major Developments and Issues in Modal Identification, Proceedings of 22nd International Modal Analysis Conference (IMAC), Detroit, USA, 2004.
[13] D. Lyon, N.C. Remedios, Resonance testing of railway vehicles, Veh. Syst. Dyn. 8 (2–3) (1979) 149, https://doi.org/10.1080/00423117908968586.
[14] T. Tomioka, T. Takigami, Experimental and numerical study on the effect due to passengers on flexural vibrations in railway vehicle carbodies, J. Sound. Vib. 343 (2015) 1–19.
[15] J. Soukup, J. Skočilas, B. Skočilasová, Assessment of railway wagon suspension characteristics, Mech. Syst. Signal Process. 89 (2017) 67–77.
[16] H.L. Shi, P.B. Wu, R. Luo, J. Zeng, Estimation of the damping effects of suspension systems on railway vehicles using wedge tests, J. Rail Rapid Transit 230 (2) (2016) 392–406.
[17] M. Dumitriu, Fault detection of damper in railway vehicle suspension based on the cross-correlation analysis of bogie accelerations, Mech. Ind. 20 (102) (2019) 1–14.
[18] L.M. Erviti, J.G. Giménez, A. Alonso, Error analysis of the application of combined subspace identification to the modal analysis of railway vehicles, J. Sound Vib. 407 (2017) 144–169.
[19] J. Zwolski, J. Bień, Modal analysis of bridge structures by means of forced vibration tests, J. Civ. Mech. Eng. Manag. 17 (4) (2011) 590–599.
[20] S. Lachinger, A. Vorwagner, M. Reiterer, J. Fink, S.-Z. Bruschetini-Ambro, Determination of dynamic properties of railway bridges through forced excitation, 39th, IABSE Symp. Eng. Fut. Vancouver (2017).
[21] D. Bacinskas, Z. Kamaitis, D. Jatulis, A. Kilikevicius, Field testing of old narrow-gauge railway steel truss bridge, Proc. Eng. 57 (2013) 136–143.
[22] C. Rebelo, M. Heiden, M. Pircher, L. Simões da Silwa, Vibration measurements on existing single-span concrete railway viaducts in Austria, EURODYN 2005, Proc. of 6th International Conference on Structural Dynamics (2005) 1637–1642.
[23] B.H. Kim, J. Lee, D.H. Lee, Extracting modal parameters of high-speed railway bridge using the TDD technique, Mech. Syst. Signal Process. 24 (2010) 707–720.
[24] O. Caglayan, K. Ozakgul, O. Tezer, Assessment of existing steel railway bridges, J. Constr. Steel Res. 69 (2012) 54–63.
[25] K. Liu, E. Reynders, G. De Roeck, G. Lombaert, Experimental and numerical analysis of a composite bridge for high-speed trains, J. Sound Vib. 320 (2009) 201–220.
[26] G. Poprawa, M. Salamak, S. Pradelok, Specific dynamic response of truss railway bridge identified using operational modal analysis as an extension of typical dynamic load testing, Proc. of International Conference on Noise and Vibration Engineering ISMA 2018 / International Conference on Uncertainty in Structural Dynamics USD 2018, 1597–1606.
[27] M. Szafrański, Dynamic analysis of the railway bridge span under moving loads. Roads and Bridges – Drogi i Mosty, 17 (2018) 299-316.
[28] W. Zhai, Z. Han, Z. Chen, L. Ling, A. Zhu, Train-track-bridge dynamic interaction: a state of the art review, Veh. Syst. Dyn. 57 (7) (2019) 984–1027, https://doi.org/10.1080/00423114.2019.1605085.
[29] K. Matsuoka, A. Collina, C. Somaschini, M. Sogabe, Influence of local deck vibrations on the evaluation of the maximum acceleration of a steel-concrete composite bridge for a high-speed railway, Eng. Struct. 200 (2019), https://doi.org/10.1016/j.engstruct.2019.109736 109736.
[30] D. Ribeiro, R. Calçada, R. Delgado, M. Brehm, V. Zabel, Finite element model updating of a bowstring-arch railway bridge based on experimental modal parameters, Eng. Struct. 40 (2012) 413–435, https://doi.org/10.1016/j.engstruct.2012.03.013.
[31] J. Malveiro, D. Ribeiro, C. Sousa, R. Calçada, Model updating of a dynamic model of a composite steel-concrete railway viaduct based on experimental tests, Eng. Struct. 164 (2018) 40–52.
[32] D. Ribeiro, R. Calçada, R. Delgado, M. Brehm, V. Zabel, Finite-element model calibration of a railway vehicle based on experimental modal parameters, Veh. Syst. Dyn. 51 (6) (2013) 821–856, https://doi.org/10.1080/00423114.2013.778416.

[33] J.N. Juang, R.S. Pappa, An eigensystem realization algorithm for modal parameter identification and model reduction, J. Guid. Control Dyn. 8 (1985) 620–627.
[34] J. Bendat, A. Piersol, Engineering applications of correlation and spectral analysis, John Wiley & Sons, Inc., 1980.
[35] M. Szafrański, Dynamics of the small-span railway bridge under moving loads, MATEC Web Conf. 262 (10014) (2019) 1–8.
[36] MATLAB, Getting started guide, The MathWorks, Inc., Natick MA, 2016.
[37] J.J. Hollkamp, R.W. Gordon, Modal test experiences with a jet engine fan model, J. Sound Vib. 248 (2001) 151–165.
[38] E. Rusinski, S. Dragan, P. Moczko, D. Pietrusiak, Implementation of experimental method of determining modal characteristics of surface mining machinery in the modernization of the excavating unit, Arch. Civ. Mech. Eng. 12 (2012) 471–476.
[39] R.D. Nayeri, F. Tasbihgoo, M. Wahbeh, J.P. Caffrey, S.F. Masri, J.P. Conte, et al, Study of time-domain techniques for modal parameter identification of a long suspension bridge with dense sensor arrays, J. Eng. Mech. (2009) 669–683.
[40] A. Tomaszewska, M. Szafrański, Study on applicability of two modal identification techniques in irrelevant cases, Arch. Civ. Mech. Eng. 20 (2020) 13.
[41] J.N. Juang, Applied system identification, Englewood Clifs: Prentice-Hall PTR, New Jersey, 1994.
[42] K.L. Johnson, Contact Mechanics. Cambridge University Press, 1985.
[43] C. Esveld, Modern Railway Track, MRT Productions, 1989.
[44] H.H. Jenkins, J.E. Stephenson, G.A. Clayton, H.W. Morland, D. Lyon, The effect of track and vehicle parameters on wheel/rail vertical dynamic forces, Railway Eng. J. 3 (1) (1974) 2–16.
[45] M. Podworna, Dynamic response of steel-concrete composite bridges loaded by high-speed train, Struct. Eng. Mech. 62 (2) (2017) 179–196.
[46] SOFiSTiK Manual, v. 2014, SOFiSTiK AG, Oberschleißheim, Germany, www.sofistik.com.
[47] M. Szafrański, Vibration of the bridge under moving singular loads - theoretical formulation and numerical solution, J. Appl. Math. Comput. Mech. 15 (1) (2016) 169–180.
[48] European Committee for Standardization, EN 1990 Basis of structural design – Annex A2: Application for bridges. CEN, Brussels, 2002.
[49] L. Fryba, Dynamics of Railway Bridges, Thomas Telford, 1996.